2014 IEEE International Conference on Robotics & Automation (ICRA)
Hong Kong Convention and Exhibition Center
May 31 - June 7, 2014. Hong Kong, China

A New Flexible Controller for a Humanoid Robot That Considers Visual and Force Information Interaction*

Gan Ma[12], Qiang Huang[123], Zhangguo Yu[12], Xuechao Chen[12],
Weimin Zhang[12], Junyao Gao[12], Libo Meng[12] and Yun-Hui Liu[14]

Abstract— **To enhance the safety of a humanoid robot when it is operating a complex environment, a number of methods that combine visual and force information have been presented. These methods are generally divided into two approaches. The first approach is to coordinate the visual controller and force controller in a parallel way, and the second approach is to coordinate them in series. However, these two approaches do not consider the interaction between the visual controller and force controller. Specifically, the first approach does not consider the interaction between the controllers. The second approach only considers the effect of the output of the visual controller on the force controller, while the effect of the force controller on the visual controller is not considered. This study presents a design for a new flexible controller for a humanoid robot that considers the interaction of visual and force information. The advantages of the proposed method are that it simultaneously incorporates the functions of a visual servo controller and a flexible controller as well as its ability to consider the interaction of visual and force information when a humanoid robot is operating.**

I. Introduction

In contrast to other robots, humanoid robots have the advantage of being able to adapt to the environment of humans because of their human-like appearance and structure [1]. Therefore, humanoid robots are more suited to serve people. In recent decades, an increasing number of researchers have been engaged in the study of humanoid robots, especially in the area of dynamic walking [2] and balance control [3]. However, there are a number of key technical issues concerning humanoid robots that remain to be solved, including the ability to accurately sense and safely operate in a complex environment.

An image capture method employing a camera, which can gather large amounts of information from the environment, is very useful for the operation of a robot. A number of researchers have proposed methods to obtain target information from the camera image and subsequently use it to control the movement of a robot [4][5]. Meanwhile, other researchers are dedicated to the study of using visual information in the dynamic feedback loop [6]-[11]. This technology is referred to as visual servoing [12][13]. The above-mentioned methods generally utilize a visual feedback method to directly control the movement of a humanoid robot. However, when a humanoid robot is operating in a complex environment, it tends to come into contact with objects it may not have noticed. In this case, the robot or the environment may become damaged if a stiffness control algorithm is adopted. Thus, pure visual servoing control cannot guarantee the safety of a humanoid robot operating in a complex environment.

To enhance the safety of humanoid robots during operation, a number of methods have been proposed. These methods combine the visual and force information to control the robot, and they are mainly divided into two approaches. The first approach coordinates the visual controller and force controller in a parallel way. Specifically, a controller coordinator is employed to coordinate the values from the visual controller and force controller. The final control values are obtained from the controller coordinator [14][15]. The second approach coordinates the visual servo controller and the force controller in series. Specifically, this approach integrates the visual servo controller and the force controller into a control loop, and the output of the visual servo controller is used as the input of the force controller. The final control values are obtained from the force controller [16]-[18]. These two approaches provide flexible methods of controlling a robot's interaction with a known environment. However, the first approach does not consider the interaction of the visual controller and force controller. In contrast, in the second approach, the visual controller is the main controller, and this approach simply considers the effect of the visual controller output on the force controller. Thus, both methods do not consider the interaction of the two controllers. In fact, when a humanoid robot performs a complex task, such as opening a door, the force controller data should also be used as feedback for the visual controller, which is essential to enhancing the accuracy of the control system.

This study focuses on the sensing and operating problem of a humanoid robot in a complex environment. In this study, a new flexible controller that considers the interaction of the visual and force information for a humanoid robot was designed. The proposed method simultaneously functions as both a visual servo controller and a flexible controller, and it can solve the above-mentioned interaction problem caused by other approaches.

The remainder of this paper is structured as follows. First, a high-precision, image-based visual servo algorithm

*This work was supported by the National Natural Science Foundation of China under Grants 61320106012, 61375103, 61273348 and 61175077, and "111 Project" under Grant B08043

[1]IRI, School of Mechatronical Engineering, Beijing Institute of Technology, Beijing, China {magan,qhuang,yuzg}@bit.edu.cn, yhliu@mae.cuhk.edu.hk

[2]Key Laboratory of Biomimetic Robots and Systems, Ministry of Education, China

[3]Key Laboratory of Intelligent Control and Decision of Complex System, China

[4]The Department of Mechanical and Automation Engineering, The Chinese University of Hong Kong, Hong Kong

for an eye-in-hand camera system is designed. Next, a new flexible controller that considers the interaction of visual and force information for a humanoid robot is designed. Finally, the task of a humanoid robotic arm approaching a certain point and drawing a circle on a board is performed by our humanoid robot platform to verify the proposed methods.

II. Modeling of a humanoid robotic arm

This section addresses the modeling of a humanoid robotic arm. Fig. 1 shows the basic structure and coordinate frames of the robotic arm. Because this study mainly focuses on the control of a humanoid robotic arm, the body of the humanoid robot is simplified as a fixed rigid base; the robotic arm is attached to the rigid base, which consists of three rigid links, and an eye-in-hand camera is mounted at the tip of the robotic arm.

The base frame Σ_b is placed at a base point of the robotic arm. The end-effector frame Σ_e is fixed at the tip of the robotic arm. Σ_c is the camera frame. In this section, the kinematic model, dynamic model and pinhole model of the robotic arm are established.

A. Kinematic Modeling of the System

The kinematic model describes motion without considering the forces that cause it. The forward kinematics of the robotic arm are

$$x_e = f(q), \tag{1}$$

where q denotes the vector of the joint angles and x_e denotes the position and attitude of the end-effector frame with respect to the base frame. In this study, the orientation of the robotic arm is denoted as three parameters using the X-Y-Z fixed angles rotation method [19], where the rotation order is $R_x(\alpha)$, $R_y(\beta)$ and $R_z(\gamma)$. In this case, x_e is defined as

$$x_e = [x\ y\ z\ \alpha\ \beta\ \gamma]^T. \tag{2}$$

The velocity kinematics describe the relation between the joint velocity $\dot{q}$ and the Cartesian velocity $\dot{x}_e$, which is defined as

$$\dot{x}_e = J_m \dot{q}, \tag{3}$$

where J_m denotes the Jacobian matrix of the robotic arm.

B. Dynamic Modeling of the System

The dynamic model of a robot describes the relation between the motion of the robot, and the forces that cause the motion. In this section, the Lagrangian method is used to model the robotic system. The robot's dynamics equations are described as follows:

$$M(q)\ddot{q} + H(q,\dot{q}) + G(q) = J_m^T F_{ext} + \tau_m, \tag{4}$$

where the left three terms denote the inertia force, Coriolis force and gravity, respectively; F_{ext} denotes external force applied to in the end-effector; and τ_m denotes the input torque of the robotic arm joints.

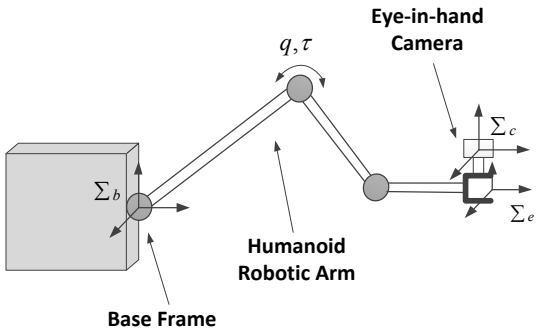

Fig. 1. Model of a humanoid robotic arm

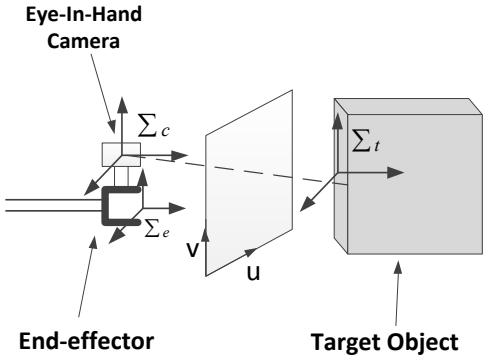

Fig. 2. Eye-in-hand vision system

C. Pinhole Model of the System

In this section, an eye-in-hand visual tracking model is constructed (Fig. 2). This paper assumes that N $(N >= 3)$ feature points are mounted on the target and that the coordinates of the feature points are already known with respect to the target frame Σ_t.

It is essential to capture the position and attitude of a target in real-time as the camera is constantly moving when the robot is manipulating an object. In this section, the perspective projection method is employed to model the eye-in-hand camera projection. In this case, the camera is a pinhole camera with a perspective projection. The 2D image frame is denoted by $\{u, v\}$. Under this model,

$$y = \frac{1}{z} P\ {}^c x_t, \tag{5}$$

where ${}^c x_t$ is the homogeneous coordinates of the feature point with respect to the camera frame, z is the depth of the feature points, $y = [u, v]^T$ is the projection coordinate of the feature points on the image plane, and P is a matrix, composed of the first two rows of the 3×4 perspective projection matrix M. The matrix M is dependent on the intrinsic and extrinsic parameters of the camera [20].

III. Eye-in-hand visual servo controller

This section proposes an algorithm for an accurate visual servo controller that can be used to control the movement of a robotic arm without external forces being applied. The objective of the control algorithm is to lock the projection of all the feature points at a desired fixed position y_d on the image plane.

The relation between the image-plane velocity of a feature point and the velocity of the point with respect to the camera frame can be described by the image Jacobian matrix

$$\dot{y} = J_{image} \begin{bmatrix} {}^{c}v_t \\ {}^{c}w_t \end{bmatrix} \tag{6}$$

where $[{}^{c}v_t, {}^{c}\omega_t]^T$ is the velocity of the feature point with respect to the camera frame and J_{image} denotes the image Jacobian matrix of the camera, which is defined as

$$J_{image} = \begin{bmatrix} \frac{\lambda}{z} & 0 & -\frac{u}{z} & -\frac{uv}{\lambda} & \frac{\lambda^2+u^2}{\lambda} & -v \\ 0 & \frac{\lambda}{z} & -\frac{v}{z} & \frac{-\lambda^2-v^2}{\lambda} & \frac{uv}{\lambda} & u \end{bmatrix}. \tag{7}$$

When N feature points are used, the extended image Jacobian is denoted by

$$J_{images} = \begin{bmatrix} J_{image1} \\ \cdot \\ \cdot \\ J_{imageN} \end{bmatrix}. \tag{8}$$

Because of the hypothesis that the desired position on the image plane y_d is constant, the desired velocity and acceleration on the image plane should be zero, which leads to the nominal reference

$$\hat{\dot{y}}_d = \dot{y}_d - \lambda \Delta y = -\lambda \Delta y, \tag{9}$$

where λ is positive scalar and Δy is 2×1 image error vector of the feature point.

In this study, we also assume that the desired end-effector of the robotic arm is moving at a constant velocity. This assumption leads to the nominal depth

$$\hat{z}_d = z - \frac{v_{ez}}{\lambda}, \tag{10}$$

where v_{ez} denotes the third row of $[v_e, \omega_e]^T$. In this case, the estimation of J_{image} is

$$\hat{J}_{image} = \begin{bmatrix} \frac{\lambda}{\hat{z}} & 0 & -\frac{u}{\hat{z}} & -\frac{uv}{\lambda} & \frac{\lambda^2+u^2}{\lambda} & -v \\ 0 & \frac{\lambda}{\hat{z}} & -\frac{v}{\hat{z}} & \frac{-\lambda^2-v^2}{\lambda} & \frac{uv}{\lambda} & u \end{bmatrix}. \tag{11}$$

The estimation of the velocities of the target relative to the camera frame are deduced from (6)

$$\begin{bmatrix} {}^{c}\hat{v}_t \\ {}^{c}\hat{\omega}_t \end{bmatrix} = K \hat{J}^{-1}_{image} \hat{\dot{y}}_d, \tag{12}$$

where K is the gain matrix, $\hat{J}^{-1}_{image}$ denotes the inverse matrix of the estimation of J_{image}, and $[{}^{c}\hat{v}_t, {}^{c}\hat{\omega}_t]^T$ denotes the estimation of the target velocities with respect to the camera frame.

We denote the desired target velocities in the camera frame as $[{}^{c}v_{td},\ {}^{c}\omega_{td}]^T$. To reach the desired target velocities, the estimation error of the end-effector of the robotic arm is denoted by $[\Delta v_e,\ \Delta\omega_e]^T$, where

$$\begin{bmatrix} \Delta v_e \\ \Delta\omega_e \end{bmatrix} = \begin{bmatrix} {}^{c}\hat{v}_t \\ {}^{c}\hat{\omega}_t \end{bmatrix} - \begin{bmatrix} {}^{c}v_{td} \\ {}^{c}\omega_{td} \end{bmatrix}. \tag{13}$$

IV. The new flexible controller for a robot

This section discusses the proposed new flexible controller, which considers the interaction of visual and force information for a humanoid robot. When the robot is operating in a complex environment, it tends to come into contact with objects it may not have noticed. In this case, a pure visual servo controller cannot guarantee the safety of the robot.

To simultaneously enhance the accuracy and the safety of the arm during operation, a model that utilizes a virtual mass-spring-damper in the end-effector of the arm is established (Fig. 3). Here, the relation between the measured interaction effort F_{ext} and the motion about the end-effector reference trajectory of the arm x_e is

$$J\ddot{x}_e + B\Delta\dot{x}_e + K\Delta x_e = F_{ext}, \tag{14}$$

where Δx_e is the displacement of the end-effector position from the reference point and $J \in R^{6\times6}$, $B \in R^{6\times6}$ and $K \in R^{6\times6}$ are the desired inertia, damping and stiffness values, respectively. For an anthropomorphic robotic arm to interact with the environment, the impedance characterization of the human arm [21] and biomechanical data [22] can help us to select the correct inertia, damping and stiffness parameters.

The controlled acceleration $\hat{\ddot{x}}$ of the system, which is based on (14), is

$$\hat{\ddot{x}}_e = J^{-1}\{F_{ext} - B\Delta\dot{x}_e - K\Delta x_e\}. \tag{15}$$

By adding (15) to (13), the total velocities of the end-effector of the robotic arm can be denoted by $[v_e,\ \omega_e]^T$, where

$$\begin{bmatrix} v_e \\ \omega_e \end{bmatrix} = \begin{bmatrix} v_{ed} \\ \omega_{ed} \end{bmatrix} + \begin{bmatrix} \Delta v_e \\ \Delta\omega_e \end{bmatrix} + \hat{\ddot{x}}_e \Delta T, \tag{16}$$

$[v_{ed},\ \omega_{ed}]^T$ are the desired velocities of the end-effector, and ΔT is the control period of the system.

Substituting (16) into (3) gives the joint velocities $\hat{\dot{q}}$ as

$$\hat{\dot{q}} = J_m^{-1} \begin{bmatrix} v_{ed} \\ \omega_{ed} \end{bmatrix} + J_m^{-1} \begin{bmatrix} \Delta v_e \\ \Delta\omega_e \end{bmatrix} + J_m^{-1} \hat{\ddot{x}}_e \Delta T. \tag{17}$$

Based on the differentiation of (17), the controller is defined as

$$\tau_m = M(q)\hat{\ddot{q}} + H(\hat{q}, \hat{\dot{q}}) + G(\hat{q}), \tag{18}$$

where τ_m is the joint control torques of the robot.

Thus, by properly selecting the constant matrices, the arm can be controlled by the proposed controller, and the end-effector of the arm can behave as a mass-damper-spring system.

The proposed approach is different from [14][15] and [16]-[18] in terms of its consideration of the interaction of visual and force information. Specifically, the previous approaches simply present methods to coordinate a visual controller and a force controller to enhance the safety of the robot while

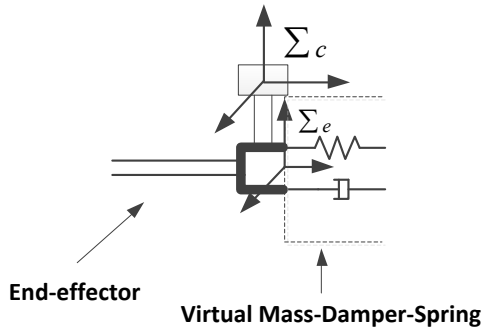

Fig. 3. Flexible model of the robotic arm

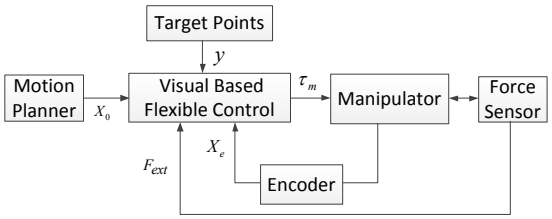

Fig. 4. The new flexible control structure

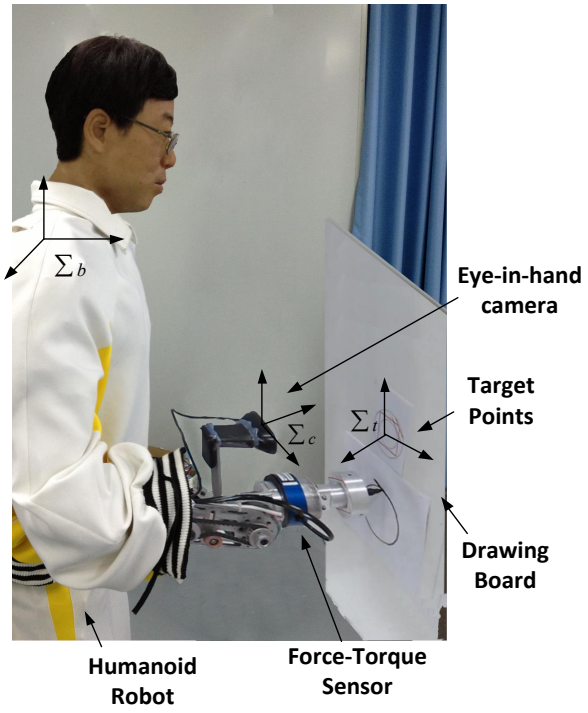

Fig. 5. The experimental platform

TABLE I
DYNAMIC PARAMETERS FOR THE ROBOTIC ARM

	$Mass\ [kg]$	$I_{xx}\ [kgm^2]$	$I_{yy}\ [kgm^2]$	$I_{zz}\ [kgm^2]$
Upper Arm	3.807	0.004865	0.001686	0.005318
Lower Arm	2.515	0.002401	0.001043	0.002732
Hand	1.078	0.001673	0.001656	0.002087

performing a task. In the proposed approach, the controller simultaneously functions as a visual servo controller and a flexible controller. The projection coordinate of the target points on the image plane y, the external forces F_{ext}, and the joint angles detected by the encoders X_e are the inputs of the controller, and these inputs are processed simultaneously in the controller. The joint control torques τ_m are the outputs of the controller. Fig. 4 shows the overall structure of the proposed flexible control method.

V. EXPERIMENTAL VERIFICATION

A. Experimental Platform

To validate the effectiveness of the proposed method, an experiment is performed using our humanoid robot BHR-4 (Fig. 5). This robot consists of a torso, head, waist, two arms and two legs. The height of the robot is 1.65 m, and it weights approximately 60 kg. This robot has 51 degrees of freedom (DOF), including 13 facial joints that produce vivid facial expressions.

Its arms have six degrees of freedom, and they are designed in an anthropomorphic way: three DOFs in the shoulder, two DOFs in the elbow and one DOF in the wrist. The length of the arm is 0.733 m, and it weights approximately 7.4 kg. The arm is divided into three parts: the upper arm with a length of 0.33 m, the lower arm with a length of 0.22 m and the end-effector with a length of 0.183 m. Table I lists the dynamic parameters of the arm. To perform our drawing task, a pen tip is designed as the end-effector of the arm. In addition, a 6-axis force/torque sensor is mounted on the end-effector and is used to detect the forces and torques caused by the drawing board. A SVS camera with a sampling rate of 15 fps is mounted on the end-effector of the arm. The base frame Σ_b is fixed at the shoulder of the arm, and the target frame Σ_t is fixed at the center of the target object. The camera frame Σ_c is fixed on the camera.

The robot is controlled by a main control computer and by joint controllers on every joint. The main control computer uses the Quick UNIX (QNX) [23] operating system to control the robot. Communication between the main control computer and the joint controllers is based on Ethernet for Control Automation Technology (EtherCAT) communication, which was developed by Bechhoff. The main control computer is the master for EtherCAT communication, while the motor controllers are the slave nodes. The control loop is set at 250 Hz.

B. Tracking Experiment

To verify the effectiveness of the proposed controller, the humanoid robotic arm is directed to approach a target board and subsequently draw a circle on the board. Five target

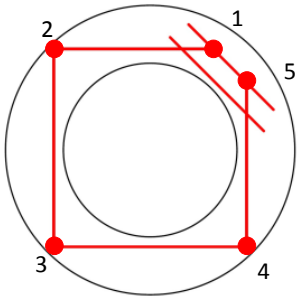

Fig. 6. Distribution of feature points

points, which are detected using computer vision techniques, are used to determine the position and attitude of the target and are distributed as shown in Fig. 6.

To perform the drawing task, this experiment is divided into two parts. First, the robotic arm adjusts its position and attitude to track the starting point of the drawing task. In this part, no external forces exist; the controller functions as a pure visual servo controller. When the tip of the robotic arm comes into contact with the drawing board, the robotic arm attempts to draw a circle. In this case, the proposed controller would simultaneously manage the information from both the camera and the 6-axis force sensor.

In the tracking experiment, the initial position and attitude of the end-effector are

$$X_{e0} = [0, 0.403, -0.33, 90°, 0°, 0°]. \tag{19}$$

The nominal position and attitude of the target are

$$X_{t0} = [0, 0.38, -0.23, 88°, -1°, -1°]. \tag{20}$$

Fig. 7 shows the variations in the position and attitude of the end-effector. Fig. 8 shows the variations in the line velocities and the angular velocities of the end-effector. Fig. 7 indicates that both the position errors and attitude errors decrease during this phase. Fig. 7 also shows that the position and attitude of the end-effector X_e gradually approach those to the starting drawing point X_{t0}. Fig. 8 indicates that the velocities are continuous and that the fluctuation is minimal.

C. Drawing Experiment

When the robotic arm is tracked to the starting drawing point X_{t0} on the drawing board, the drawing task is performed. In this experiment, the controller receives information from both the camera and the force sensor.

TABLE II

LENGTH ERRORS ON THE DRAWING BOARD

Numbers	1	2	3	4	5	6	7	8	9	10
ΔL $[mm]$	3.2	2.4	1.8	2.7	0.4	1.9	1.5	1.8	2.3	0.7

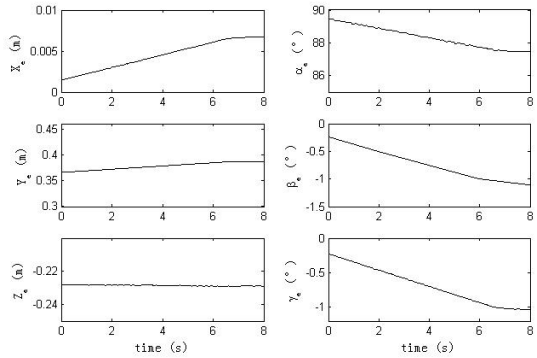

Fig. 7. Position and attitude of the end-effector during tracking

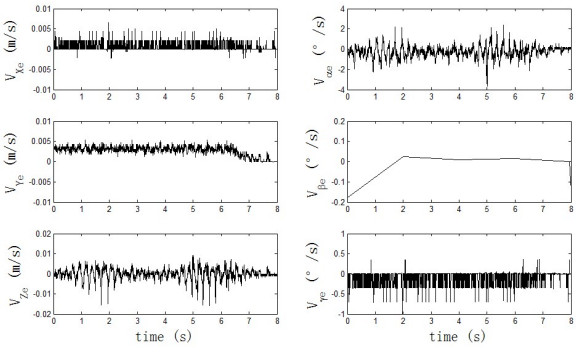

Fig. 8. Velocities of the end-effector during tracking

In this experiment, the robot attempts to draw a circle with a radius of 0.04 m on the drawing board. Fig. 9 shows the variations in the position and attitude of the end-effector, and Fig. 10 shows the variations in the velocities of the end-effector during the drawing task.

As shown in Fig. 9 and Fig. 10, the position and attitude of the tip of the arm change during the task but finally converge to the starting drawing point. Fig. 9 shows that the attitude of the arm remains approximately constant during this phase. The attitude remains approximately constant because the robot is controlled to maintain the same attitude vertical to the drawing board during the drawing task. Fig. 10 indicates that the arm is moving smoothly.

To validate the accuracy of the proposed method, the experiments are performed ten times, and each time, the target drawing board is placed in different positions with different attitudes. This process creates different camera information and force sensor information inputs for the controller. Table II shows the length errors ΔL between the desired final point and the actual final point on the drawing board. A statistical analysis shows that the system has relatively low error, which indicates that the proposed controller performs well.

VI. CONCLUSION

This study focused on the problem of accurate sensing and safe operation of a humanoid robot in a complex environment. The contributions of this paper are as follows:

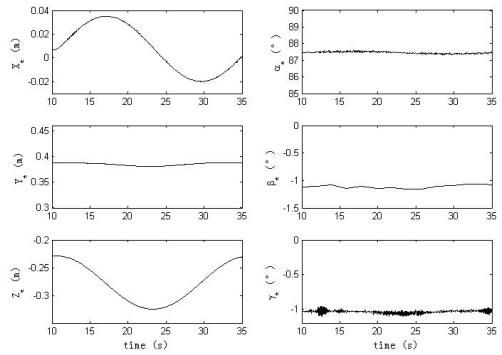

Fig. 9. Position and attitude of the end-effector during the drawing task

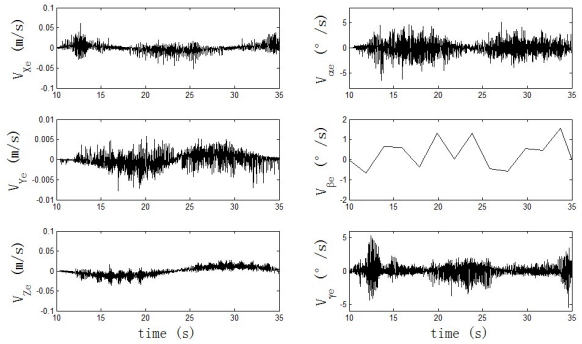

Fig. 10. Velocities of the end-effector during the drawing task

1) A new flexible controller that considers the interaction of visual and force information for a humanoid robot is designed.

2) The advantages of the proposed method are that it simultaneously functions as a visual servo controller and flexible controller, and it also considers the interaction of visual and force information when a humanoid robot is operated.

3) The proposed method was validated on a humanoid robotic platform.

For a humanoid robot to operate when walking, it is crucial to guarantee the dynamic stability of the robot. The whole-body motion dynamics should be considered [24][25]. This is a difficult task because the robot's balance control is a challenging problem when planning the whole-body movement of a humanoid robot on-line. Our future study will focus on the whole-body movement of a humanoid robot when operating in an unpredictable environment.

REFERENCES

[1] D. Sakamoto, T. Kanda, and T. Ono, "Cooperative embodied communication emerged by interactive humanoid robots," *International Journal of Human-Computer Studies*, vol. 62, no. 2, pp. 247-265, 2005.

[2] M. F. Silva, and J. A. T. Machado, "A literature review on the optimization of legged robots," *Journal of Vibration and Control*, vol. 18, no.12, pp. 1753-1767, 2012.

[3] C. Y. Chen, and P. H. Huang, "Review of an autonomous humanoid robot and its mechanical control," *Journal of Vibration and Control*, vol. 18, no.7, pp. 973-982, 2012.

[4] J. Kim, I. Park, J. Lee, and J. Oh, "Experiments of vision guided walking of humanoid robot, KHR-2," *IEEE International Conference on Humanoid Robots*, pp. 135-140, 2005.

[5] N. Oda, and J. Yoneda, "Visual feedback control based on optical flow vector field for biped walking robot," *IEEE International Conference on Mechatronics*, pp. 635-640, Vicenza, VI, Italy, 2013.

[6] P. Michel, J. Chestnutt, S. Kagami, K. Nishiwaki, J. Kuffner, T. Kanade, "Motion Planning Using predicted Perceptive Capability," *International Journal of Humanoid Robotics (IJHR)*, vol. 6, no. 3, pp. 435-457, 2009.

[7] P. Michel, J. Chestnutt, S. Kagami, K. Nishiwaki, J. Kuffner, T. Kanade, "GPU-accelerated real-time 3D tracking for humanoid locomotion and stair climbing," *IEEE International Conference on Intelligent Robots and Systems (IROS)*, pp. 463-469, 2007.

[8] C. Dune, A. Herdt, O. Stasse, P.-B. Wieber, K. Yokoi, E. Yoshida, "Canceling the sway motion in visual servoing for dynamic walking in visual servoing," *IEEE International Conference on Intelligent Robot and Systems (IROS)*, pp. 3175-3180, 2010.

[9] N. Mansard, O. Stasse, F. Chaumette, K. Yokoi, "Visually-Guided Grasping while Walking on a Humanoid Robot," *IEEE International Conference on Robotics and Automation (ICRA)*, pp. 3041-3047, 2007.

[10] O. Stasse, B. Verrelst, A. Davison, N. Mansard, F. Saidi, B. Verborght, C. Esteves, K. Yokoi, "Integrating Walking and Vision to increase Humanoid Autonomy," *International Journal of Humanoid Robotics*, vol. 5, no. 9, 2008.

[11] G. Taylor, L. Kleeman, "Hybrid position-based visual servoing with online calibration for a humanoid robot," *IEEE International Conference on Intelligent Robots and Systems (IROS)*, pp. 686-691, 2004.

[12] F. Chaumette, S. Hutchinson, "Visual servo control, Part I: Basic approaches," *IEEE Robotics and Automation Magazine*, vol. 13, no. 4, pp. 82-90, 2006.

[13] S. Hutchinson, G. D. Hager, and P. I. Corke, "A Tutorial on Visual Servo Control," *IEEE Transactions On Robotics and Automation*, vol. 12, pp. 651-670, 1996.

[14] B. J. Nelson, J. D. Morrow, P. Khosla, "Improved Force Control Through Visual Servoing," *American Control Conference*, pp. 380-386, 1995.

[15] K. Hosoda, K. Igarashi, M. Asada, "Adaptive Hybrid Visual Servoing/Force Control in Unknown Environment," *IEEE International Conference on Intelligent Robots and Systems (IROS)*, pp. 1097-1103, 1996.

[16] G. Morel, E. Malis, S. Boudet, "Impedance based coimbination of visual and force control," *IEEE International Conference on Robotics and Automation (ICRA)*, pp. 1743-1748, 1998.

[17] V. Lippiello, B. Siciliano, L. Villani, "Robot Interaction Control Using Force and Vision," *IEEE International Conference on Intelligent Robots and Systems (IROS)*, pp. 1470-1475, 2006.

[18] V. Lippiello, B. Siciliano, L. Villani, "A Position-Based Visual Impedance Control for Robot Manipulators," *IEEE International Conference on Robotics and Automation (ICRA)*, pp. 2068-2073, 2007.

[19] J. J. Craig, *Introduction to Robotics: Mechanics and Control*, 3rd Edition, Pearson Prentice Hall, 2005.

[20] D. Forsyth, J. Ponce, *Computer Vision: A Modern Approach*, Upper Saddle River, NJ: Prentice Hall, 2003.

[21] J. M. Dolan, M. B. Friedman, and M. L. Nagurka, "Dynamic and Loaded Impedance Components in the Maintenance of Human Arm Posture," *IEEE Transactions on Systems, Man, and Cyberbetucs*, vol. 23, no. 3, pp. 698-109, 1993.

[22] M. Kallmann, "Analytical inverse kinematics with body posture control," *Computer Animation and Virtual Worlds*, vol. 19, pp. 79-91, 2008.

[23] A. Kavas and D. G. Feitelson, "Comparing Windows NT, Linux, and QNX as the basis for cluster systems," *Concurrency Computation Practice and Experience*, vol. 13 (Compendex), pp. 1303-1332, 2001.

[24] L. Sentis and O. Khatib, "Synthesis of Whole-body Behaviors Through Hierarchical Control of Behavioral Primitives," *International Journal of Humanoid Robotics (IJHR)*, vol. 2, no. 4, pp. 505-518, 2005.

[25] N. Mansard, "A Dedicated Solver for Fast Operational-Space Inverse Dynamics," *IEEE International Conference on Robotics and Automation (ICRA)*, pp. 4943-4949, 2012.